Effect of Processing Conditions on the Yield and Failure Response of an Aliphatic Polyketone Terpolymer

NICOLE R. KARTTUNEN, ALAN J. LESSER

Polymer Science and Engineering Department, University of Massachusetts, Amherst, Massachusetts 01003

Received 21 May 2001; accepted 23 July 2001

ABSTRACT: The effect of processing conditions on the yield and failure behavior of an aliphatic polyketone terpolymer was studied. Testing and characterization were performed on samples that were extruded in the form of hollow cylinders. We performed the extrusion process at different shear rates and at different cooling rates to assess the effect that process conditions had on the polymer properties. We performed biaxial testing on the samples to characterize the failure envelopes, including the ductile–brittle transition condition for each process condition. The effect of shear rate was negligible, whereas the cooling rate significantly affected the failure behavior. To explain these differences in behavior, we performed characterization via differential scanning calorimetry, wide-angle X-ray diffraction, attenuated total reflection IR spectroscopy, dynamic mechanical thermal analysis, scanning electron microscopy, and residual stress measurements. A broad glass transition was found for all samples at temperatures higher than previously reported for this material. Alteration of the processing conditions did not influence the crystalline phase (percentage crystallinity, crystalline orientation, crystallite size, etc.). A change in spherulitic structure was also observed with altered cooling rate and is suggested to have contributed to the change in failure behavior. Residual stresses also affected the behavior of all samples. © 2002 John Wiley & Sons, Inc. J Appl Polym Sci 84: 318–334, 2002; DOI 10.1002/app.10334

Key words: polyketone; biaxiality; failure; yielding

INTRODUCTION

It is well known that processing conditions can influence the final properties of polymers. Shear stress, crystallization temperature, cooling rate, and so on are all relevant to the properties of the end product. Such processing parameters can influence the degree of orientation, impart residual stresses, and alter the degree of crystallinity. These physical changes can, in turn, affect the yield strength, stiffness, ductile–brittle transition, fracture toughness, and so on. These issues become extremely important for materials that are sensitive to processing conditions, such that slight changes in mold conditions or part design can have detrimental effects on the part performance. In this article, we present the effect that alterations in the extrusion shear rate and thermal history had on the yield and failure mode of a new semicrystalline thermoplastic. To relate these effects to morphological changes, we used various characterization techniques to examine the structure of the samples.

It has been found in various studies that shear rate is one processing parameter than can dramatically influence the properties and behavior of a material. In an injection-molding study conducted on polyethylene terepthalate (PET),[1] as

Correspondence to: A. J. Lesser.

Journal of Applied Polymer Science, Vol. 84, 318–334 (2002)

the injection speed was increased the tensile and flexural strengths decreased. It is also known that shear stress can increase crystallization kinetics[2] and induce preferred orientation during crystallization. Extremely high shear rates can also lead to degradation of the polymer. These effects can certainly influence the final material behavior.

Similarly, thermal history can significantly affect the properties of polymers through effects on the crystalline structure and free volume. In the same study by Mathew et al.,[1] it increasing cooling rate led to an increase in the yield and flexural strength of PET. A separate study on isotactic polypropylene (iPP)[3] also showed that increasing the cooling rate leads to an increased yield strength and an increased elongation at break. Additionally, the ductile–brittle transition temperature decreased with increasing cooling rate. The method used to measure this transition was not clear. In this case, the modulus was reported to change only slightly, although the trend was to increase. A more recent study of polypropylene (PP)[4] also found that increases in the cooling rate led to an increased yield strength and more ductile behavior. On the other hand, in this study of PP, the modulus increased initially and then decreased with increasing cooling rate.

It is of interest to relate changes in behavior to structural changes within the polymer. In the study by Greco and Coppola,[3] the increases in yield strength and elongation at break were accompanied by decreases in lamellar thickness and spherulite diameter. Earlier work on polyethylene indicated an increase in impact strength with cooling rate, which was connected to a decrease in spherulite size.[5] In contrast, a separate study[6] on the effect of nylon 66 spherulite size, altered by the addition of a nucleating agent, found that variation in spherulite size did not affect the impact, hardness, fatigue, or creep properties. The decrease in spherulite size increased the yield strength and modulus and decreased the percentage elongation. These results were not a result of foreign particles alone.

In other studies, increases in impact strength with the cooling rate of polycarbonate[7,8] have been linked with residual stresses. These stresses may be induced during processing due to the inability of the material to contract while cooling and are independent of induced orientations. Although residual compressive stresses have been found to increase toughness, residual tensile stresses are believed to promote brittle failures.

With regard to the specific polymer investigated here, it has previously been determined that the cooling procedure used during processing can affect properties. This has been found for barrier properties[9] and is speculated to be related to changes in crystallinity and crystal size.[10] It was, therefore, expected that differences in properties due to the cooling rate may have been detected in this study as well.

The purpose of this work was to examine the effects that various extrusion conditions had on the yield and failure response of an aliphatic polyketone terpolymer. We performed testing under biaxial loading conditions to elucidate the effect of the stress state. Additionally, we performed physical characterization of the different samples to link these effects to morphological changes and residual stresses resulting from the process conditions.

EXPERIMENTAL

Material

The material studied was an aliphatic polyketone terpolymer with the following chemical formula:

$$—(CH_2—CH_2—CO)_m—(CH_2—CHCH_3—CO)_n—$$

with $m : n$ of approximately 14 : 1. The melting temperature (T_m) was about 225°C, and the glass-transition temperature (T_g) was reported to be about 12°C.[11] The molecular weight of the material was approximately 100,000 g/mol. Samples were received in the form of extruded hollow cylinders with a diameter of approximately 22 mm and a wall thickness of approximately 2 mm from Shell Chemical Co. Five separate samples were prepared under different extrusion conditions. As a basis for comparison, the first sample was extruded under standard conditions (i.e., conditions typical for this material). This material was designated as the moderate shear rate, moderate cooling rate (MSMC) sample. Two samples were processed at either a higher or lower extrusion rate than the MSMC sample. These materials were designated at high shear rate, moderate cooling rate (HSMC) and low shear rate, moderate cooling rate (LSMC) samples. The final two samples were cooled at rates higher and lower than the standard and were designated as the moderate shear rate, high cooling rate (MSHC) and moderate shear rate, low cooling rate (MSLC)

samples. Due to proprietary reasons, further details about the processing conditions were not provided by the manufacturer. However, the conditions were chosen as practical limits over which this material could be processed, therefore, resulting in the range of properties most likely to be observed in commercial applications.

Our initial intent was to extrapolate process conditions and, thereby, the morphology of the MSMC material with the morphologies of the additional four samples; however, it is later shown that this was not the case. This was likely due to the fact that the MSMC material was processed at a different site than the other four samples. Accordingly, differences beyond just the processing parameters (polymer batch, stabilizer package, etc.) were possible. It is important to keep this in mind when the samples in this study are compared.

Biaxial Testing

The material was tested under biaxial loading conditions by simultaneous application of an axial load (tensile or compressive) and internal pressure. The specimen preparation and testing procedure was the same as described in a previous article.[12] Testing was performed under pseudo strain-rate control at a constant nominal octahedral shear strain rate ($\dot{\gamma}^{oct}$) of 0.05 min^{-1} at 20°C. $\dot{\gamma}^{oct}$ can be defined in cylindrical coordinates as

$$\dot{\gamma}^{oct} = \frac{1}{3}\sqrt{(\dot{\varepsilon}_r - \dot{\varepsilon}_z)^2 + (\dot{\varepsilon}_z - \dot{\varepsilon}_\theta)^2 + (\dot{\varepsilon}_\theta - \dot{\varepsilon}_r)^2} \quad (1)$$

where $\dot{\varepsilon}_r$, $\dot{\varepsilon}_z$, and $\dot{\varepsilon}_\theta$ are the radial, axial, and circumferential strain rates. In describing the yield response of the material in this study, we used the following convention: ductile yield was determined as the achievement of a zero-slope condition in the volumetric strain, ε_v, versus octahedral shear stress, τ^{oct}, data. For this case of biaxial loading conditions, these quantities can be calculated from the following equations:

$$\varepsilon_v = \varepsilon_r + \varepsilon_z + \varepsilon_\theta \quad (2)$$

$$\tau^{oct} = \frac{1}{3}\sqrt{(\sigma_z - \sigma_\theta)^2 + (\sigma_z)^2 + (\sigma_\theta)^2} \quad (3)$$

where ε_r, ε_z, and ε_θ are the principal strains in the radial, axial, and circumferential directions, respectively, and σ_z and σ_θ are the principal stresses in the axial and circumferential directions, respectively. Thus, if a zero-slope condition in the stress–strain curve is achieved during loading, the failure is assigned a ductile failure. If not, the failure is assigned as brittle.

Residual Stress

Residual stress calculations were made following a method described by Clutton and Williams[13] and briefly summarized here. The cylindrical samples were cut into sections of different lengths. Length-wise slices were removed from each section so that relaxation was able to occur. Because the T_g of the material was close to room temperature, we heated the samples at 100°C for 1 h to put the samples more significantly above the T_g and to allow relaxation to occur more rapidly. Following the model, measurements of the ring-closure, δ_θ, were plotted against a specimen dimension function, $F(\beta L)$, for each sample. These values were calculated from specimen dimensions and material properties as follows:

$$\delta_\theta = -\pi(D_0 - D_f) \quad (4)$$

$$F(\beta L) = \frac{2[\cos h(\beta L) - \cos(\beta L)]}{\beta L[\sin h(\beta L) - \sin(\beta L)]} \quad (5)$$

$$\beta^4 = 12\,\frac{(1 - \nu^2)}{D_0^2 h^2} \quad (6)$$

where D_0 is the initial diameter, D_f is the diameter after relaxation, L is the length of the cylinder, ν is Poisson's ratio, and $\boldsymbol{t}$ is the cylinder wall thickness. The slope, m, and intercept, c, were determined for each of the plots. Values for residual stress were then calculated for each sample with the following equations:

$$\sigma_z = -\frac{Etm}{\pi\nu D_0^2} \quad (7)$$

$$\sigma_\theta = -\frac{Etc}{\pi D_0^2} \quad (8)$$

where E is the tensile modulus. This method assumes a linear stress profile in the material, and the stresses determined are the residual stresses on the bore of the pipe specimen. This is an approximation of the actual stress distribution that allows for simplification of the analysis. The values for ν (0.40) and E (1.40 GPa) were obtained from previously performed standard tensile tests

(ASTM D-638), which were carried out at 20°C at an extension rate of 50 mm/min.

Characterization

To determine the crystallinity of the materials, we performed calorimetry work. This was carried out in a DuPont 2910 differential scanning calorimeter at a scanning rate of 10°C/min. Calculations were based on a crystalline heat of fusion of 227 J/g.[11] In another set of experiments, differential scanning calorimetry (DSC) scans were run on the MSLC and MSHC samples at a heating rate of 2°C/min.

The densities of the materials were determined via a density gradient column consisting of carbon tetrachloride and heptane. The density values were then used as a second means of determining the crystallinity of the samples with the following equations:

$$\phi_v = \frac{\rho_s - \rho_a}{\rho_c - \rho_a} \tag{9}$$

$$\phi_m = \frac{\rho_c}{\rho_s}\,\phi_v \tag{10}$$

where ϕ_v and ϕ_m are the percentage crystallinity by volume and mass, respectively, and ρ_s, ρ_a, and ρ_c are the density values of the sample, amorphous phase, and crystalline phase, respectively. Values for ρ_a and ρ_c were taken from Lommerts et al.[14] (ρ_a = 1.21 g/cm^3; ρ_c = 1.297 g/cm^3). The value of the crystalline density was for the β crystalline phase of the polyketone, as this was the dominant crystal phase for the terpolymer.[14–16]

Wide-angle X-ray diffraction (WAXD) was used to determine the crystalline orientation in the as-received samples. Pinhole collimated, monochromatic CuK_α radiation was used. Patterns were collected on a Brucker GADDS detection system.

Attenuated total reflection infrared (ATR-IR) spectroscopy was also used to characterize sample orientation. A PerkinElmer System 2000 Fourier transform IR instrument was used with a KRS crystal. The polarization was maintained in the vertical position, and spectra were obtained with the sample axial direction oriented parallel and perpendicular to the polarizer direction. Because all samples had rounded surfaces, sections with flat surfaces had to be cut. This was done with an optical microtome on samples that are chilled with liquid nitrogen. The direction of the cut was parallel with the extrusion direction. The peak height value at 1690 cm^{-1} was recorded in both the parallel and perpendicular orientations. This peak corresponded to the carbonyl stretching band[17] and, therefore, corresponded to a vibration perpendicular to the chain. The value for the average angle between the extrusion direction and local molecular chain axis, θ, was calculated for each sample from the orientation function, f:

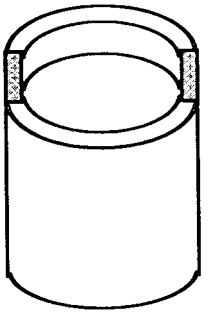

Figure 1 Schematic of the surface examined with SEM. The shaded surface is that which was examined.

$$f = \frac{3(\cos^2\theta) - 1}{2} \tag{11}$$

and also

$$f = \frac{(R - 1)(R_0 + 2)}{(R + 2)(R_0 - 1)} \tag{12}$$

where R is the dichroic ratio of the absorbance values with parallel and perpendicular sample orientations, $A_\parallel$ and $A_\perp$, respectively:

$$R = \frac{A_\parallel}{A_\perp} \tag{13}$$

and R_0, is the dichroic ratio for perfect uniaxial order

$$R_0 = 2\,\cot^2\phi. \tag{14}$$

where ϕ is the angle between the chain axis and the transition moment of the vibration that is under consideration. See, for example, Koenig.[18] For the analysis performed here, it was assumed that the transition moment of the carbonyl

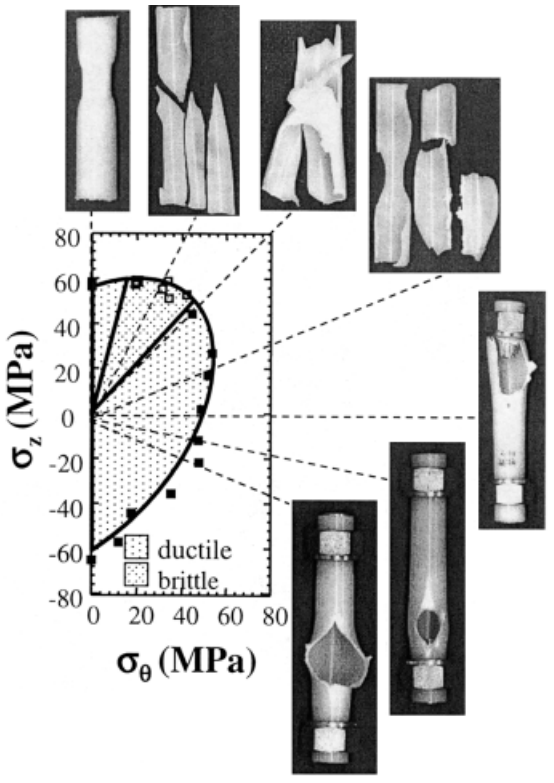
80
60
40
20
0
-20
-40
-60
-80
σz (MPa)
ductile
brittle
0 20 40 60 80
σθ (MPa)

(a)

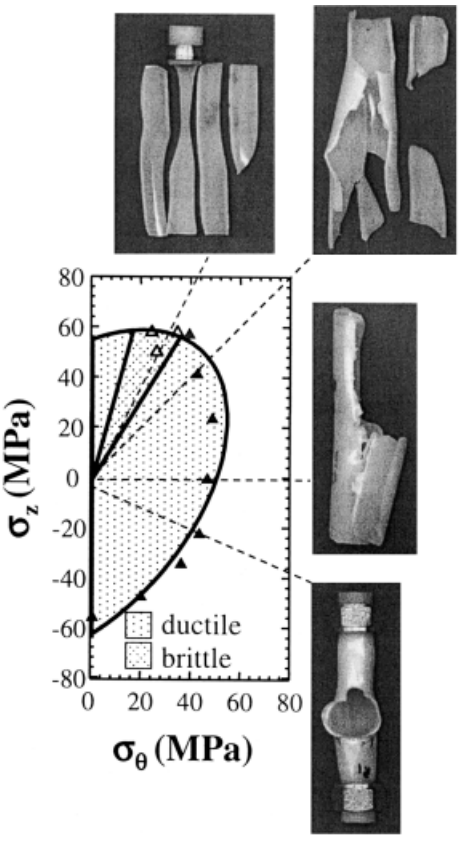
80
60
40
20
0
-20
-40
-60
-80
σz (MPa)
ductile
brittle
0 20 40 60 80
σθ (MPa)

(b)

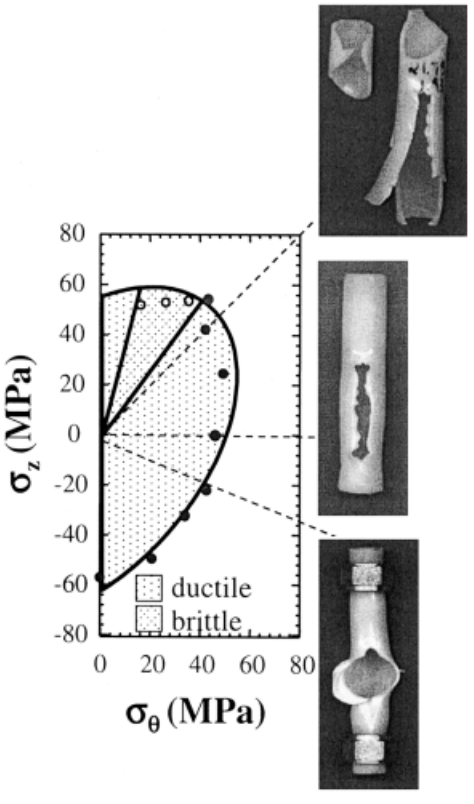
80
60
40
20
0
-20
-40
-60
-80
σz (MPa)
ductile
brittle
0 20 40 60 80
σθ (MPa)

(c)

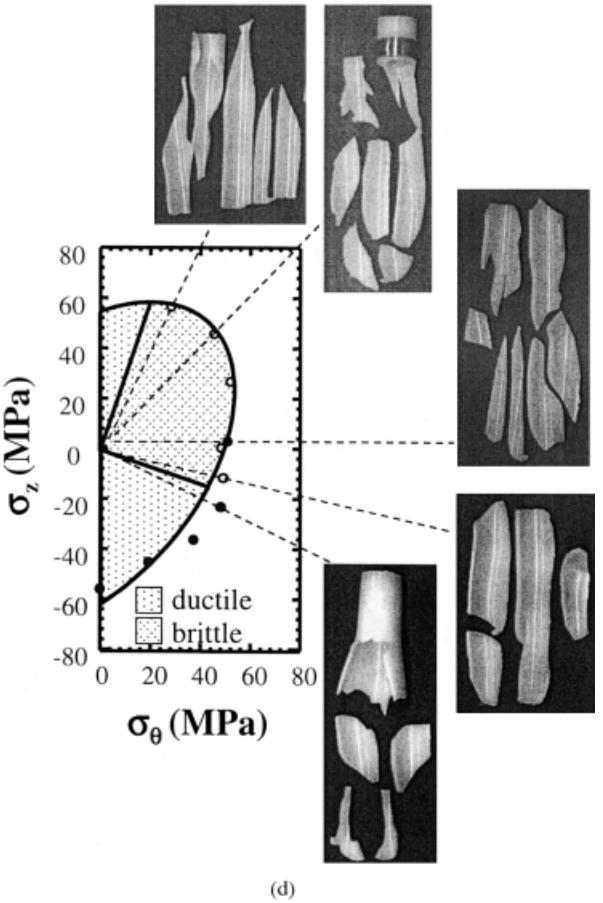
80
60
40
20
0
-20
-40
-60
-80
σz (MPa)
ductile
brittle
0 20 40 60 80
σθ (MPa)

(d)

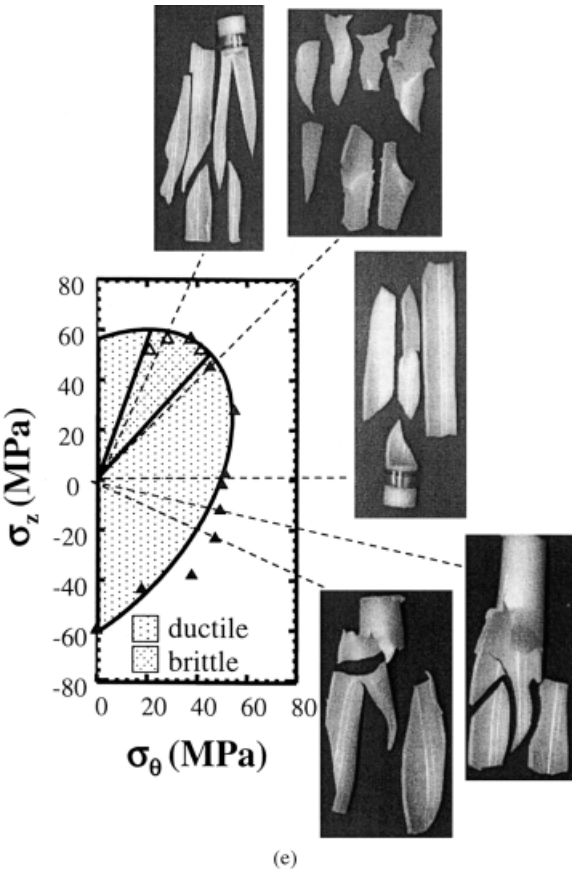

Figure 2 σ_z, versus σ_θ data and postfailure images of materials: (a) MSMC, (b) HSMC, (c) LSMC, (d) MSLC, and (e) MSHC. Lines correspond to the loading path for the respective specimen. Solid and hollow symbols represent ductile and brittle failures, respectively.

stretching band was 90° to the chain axis. Therefore, R_0 was approximated to be zero.

Scanning electron microscopy (SEM) was carried out on a JEOL 35 scanning electron microscope at 20 kV. To prepare samples, we cut sections from the hollow cylinders in a manner that allowed examination of the spherulitic structure along the length of the cylinder as well as through the wall thickness. This surface is indicated in Figure 1. The desired surface was then cut smooth on a Reichert ultracut FC4 cryomicrotome with liquid nitrogen as the cooling fluid. To provide topographical contrast, we etched the samples in a potassium permanganate/phosphoric acid etch. This procedure was developed specifically for this polymer and was described in detail elsewhere.[19] The etched samples were then mounted and gold-coated in a Polaron ES100 sputter coater.

Dynamic mechanical thermal analysis (DMTA) was carried out on a Rheometrics Mark IV dynamic mechanical thermal analyzer. All tests were performed in single-cantilever bending mode at a frequency of 1 Hz and a dynamic strain of 0.05%. Samples were cut from the cylindrical samples on a wafer saw with the cut direction parallel to the axial direction. We used samples with thickness of about 2 mm to minimize curvature in the specimens due to the cylindrical geometry. All samples were gripped to a torque value of 30 cm-N.

RESULTS AND DISCUSSION

Biaxial Testing

Figure 2(a) displays some typical specimen failures of the MSMC material over a range of stress states. This figure shows a dashed line for each specimen corresponding to the respective loading path on the schematic yield locus (σ_θ vs. σ_z). Macroscopically, a wide range of ductility was observed for this material, depending on the stress state applied to the sample. For example, specimens tested with a compressive axial stress component appeared quite ductile. With the exception of uniaxial tension, as the axial component became tensile, the failures appeared to become more brittle. This was evident because much energy was dissipated through the creation of new surface area rather than irreversible deformation of this polymer. For example, at the stress state in which the axial component was twice that of the circumferential component, the specimen shattered into fragments that could essentially be reassembled together to reform the original shape. Little energy was expended in imposing large irreversible deformation that is characteristic of ductile failures. This failure was clearly brittle. In other stress states, the mode of failure contained both ductile and brittle evidence from visual inspection. The case of equal axial and circumferential applied stress components was one such case. In this specimen, both irreversible deformation and creation of new surface area could be observed, which indicated both ductile and brittle characteristics.

Similar to the MSMC materials, the additional four materials displayed a range of ductility depending on the stress state, Figure 2(b–e). Again, mode of failure was not clear from visual inspection. For this reason, the zero-slope condition in the τ^{oct} versus ε_v curve was chosen as the criteria for ductile or brittle failure. Again, ductile failure

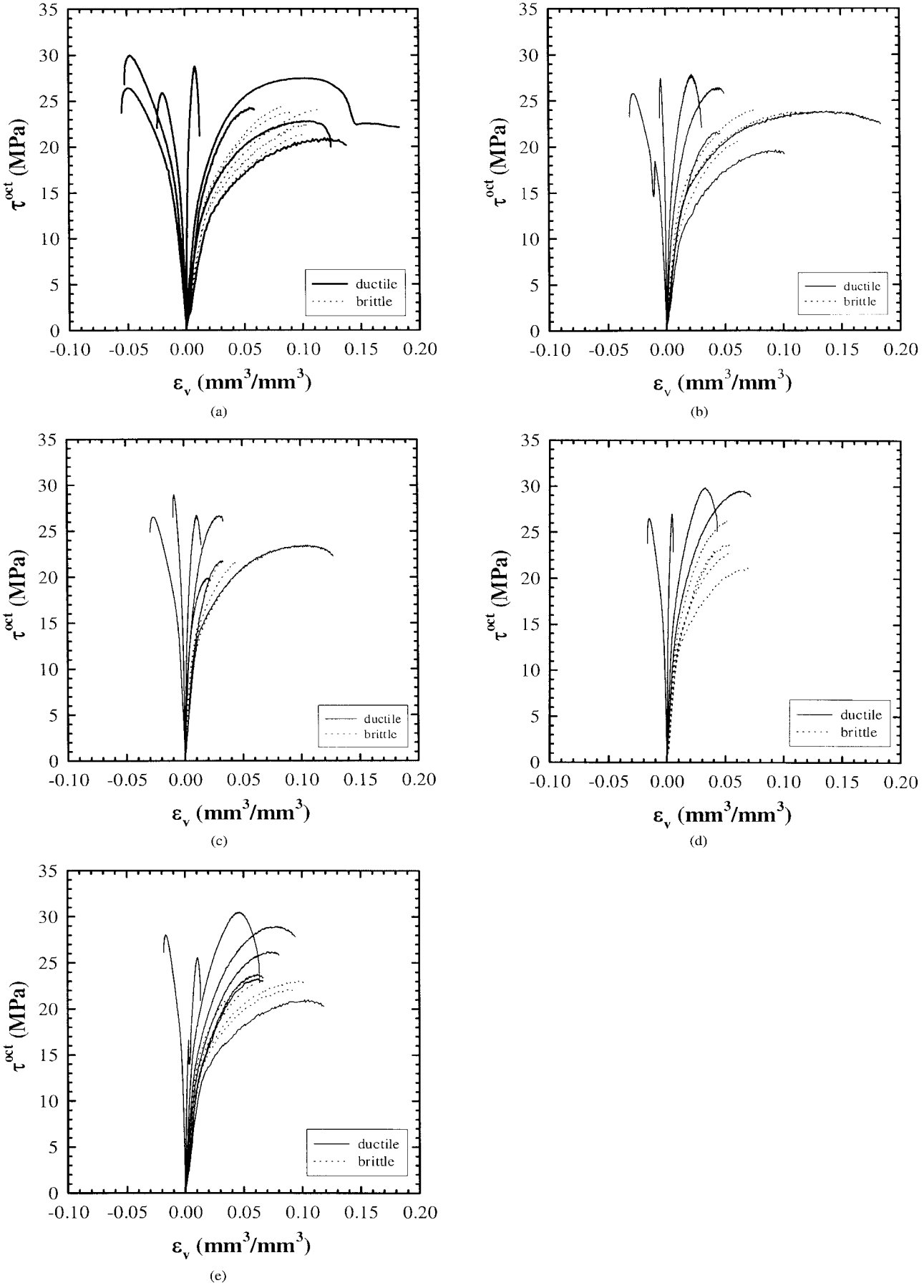

Figure 3 Octahedral shear stress as a function of volumetric strain for the (a) MSMC, (b) HSMC, (c) LSMC, (d) MSLC, and (e) MSHC materials.

was characterized by achievement of a slope value of zero in the ε_v versus τ^{oct} curve and brittle failure was characterized as nonachievement. These stress–strain curves are plotted in Figure 3(a–e).

Using the previous criteria, the yield locus of each material in Figure 2(a–e) was divided into the regions that resulted in ductile failures or brittle failures. In Figure 2, solid and hollow symbols represent ductile and brittle failures, respectively. Comparatively, the size and location of the brittle region for the high, moderate, and low shear rate materials were quite similar. Thus, the shear rate appeared to have little effect on the

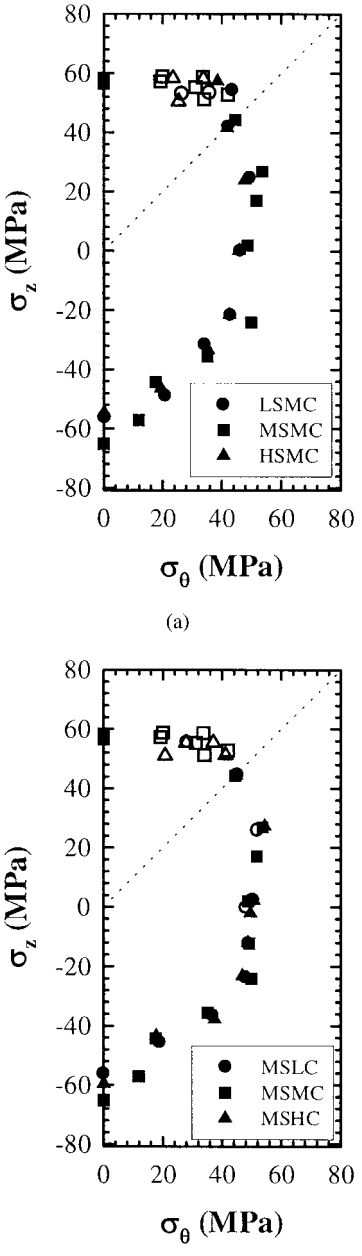

Figure 4 σ_z, σ_θ for samples processed at different (a) shear and (b) cooling rates. The dashed line indicates the case of equibiaxial loading, and solid and hollow symbols represent ductile and brittle failures, respectively.

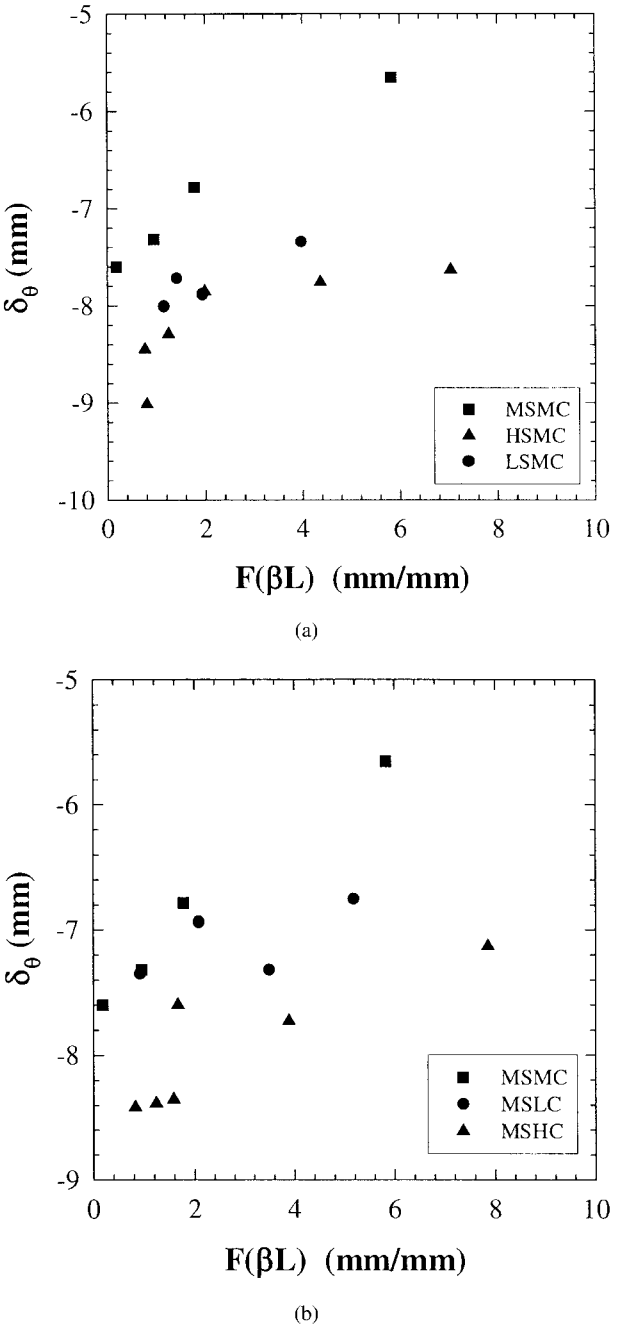

Figure 5 δ_θ versus $F(\beta L)$ used in calculation of residual stresses for samples processed at different (a) shear and (b) cooling rates.

Table I Residual Stress Values Calculated for Each Sample

Sample	σ_θ (MPa)	σ_z (MPa)
MSMC	15.7	1.7
HSMC	16.9	0.2
LSMC	16.5	0.5
MSLC	16.8	0.6
MSHC	18.6	0.8

ductile–brittle transition of this material. In contrast, the cooling rate dramatically influenced the ductile–brittle behavior. As the cooling rate decreased, the size of the brittle regime significantly increased.

It is surprising that in all the materials, brittle failures occurred in stress states that were essentially axial tension with a slight amount of internal pressure. In axial tension, ductility was clearly observed and was illustrated by the formation of a necked region. However, when the stress state was changed slightly by the simultaneous application of an axial load and a small amount of internal pressure, the samples shattered in a very brittle manner. Curiously, when the state of stress applied to a sample was the more demanding state of equibiaxial tension, which was achieved with an even greater level of internal pressurization, ductile failures were observed in four of the five materials. This was contrary to what would be expected because this stress state results in the highest levels of volumetric strain and would be expected to be the most likely to produce a brittle response. In our study, the slowly cooled MSLC material was the only sample that displayed brittle behavior in equibiaxial tension. The explanation for this interesting observation is given in the next section.

Figure 4(a,b) shows σ_a, versus σ_θ data for all samples, allowing for the direct comparison of the yield strength of samples processed under the various conditions. The results indicate that the processing conditions examined here had very little effect, if any, on the yield strength of the various samples.

To summarize, the shear rate had little effect on the material behavior. However, the thermal history affected the material behavior by increasing the size of the brittle regime as the cooling rate decreased. Neither of the processing conditions seemed to affect the yield strength of the material significantly. In all cases, except the MSLC material, ductile failure was observed in the most demanding stress state, equibiaxial tension, whereas brittle failures occurred in less demanding stress states.

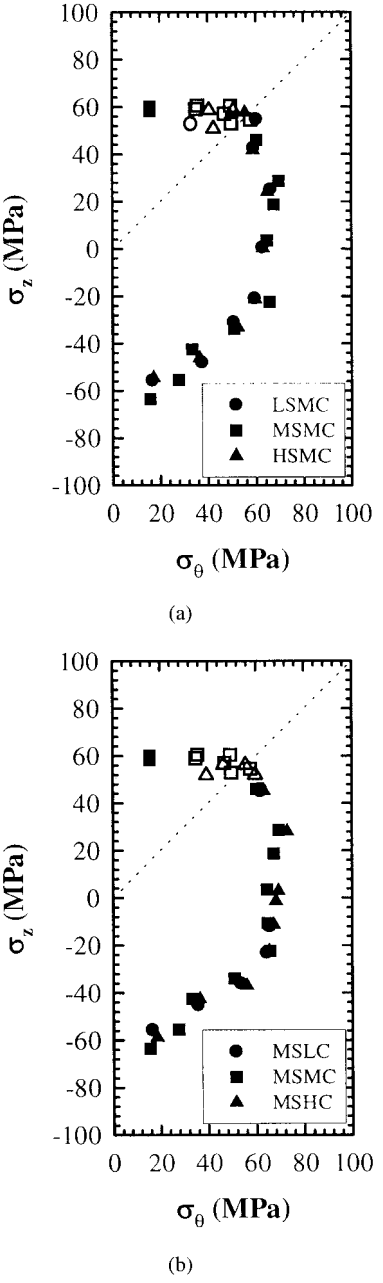

Figure 6 σ_z versus σ_θ for samples processed at different (a) shear and (b) cooling rates, shifted to account for residual stresses. The dashed line indicates the case of equibiaxial loading, and solid and hollow symbols represent ductile and brittle failures, respectively.

Residual Stress Measurements

The data used in residual stress calculations are plotted in Figure 5(a,b). The residual stress values calculated for each sample are presented in Table I. These are tensile rather than compressive stresses, which would be negative values. For all samples, the residual stress in the circumferential direction was significant, whereas the residual stress in the axial direction was quite low. As expected, the level of residual stress was greater in the rapidly cooled MSHC material than in the slowly cooled MSLC material. However, the values were not significantly different from the other samples and, therefore, did not explain why the MSLC material displayed the more brittle behavior. There was no significant change in residual stress with extrusion rate.

During testing, the applied stresses were superposed on the existing residual stresses. Therefore, the actual stress state was the combined effect of residual and applied stresses. Whereas Figure 4(a,b) indicates only the applied stresses, Figure 6(a,b) indicates the effect of shifting the data to include the calculated residual stresses. Again, the dashed line indicates the condition of equibiaxial tension, for which we expected brittle behavior but observed ductile behavior. It was observed that after this adjustment, the failures that were classified as brittle did indeed correspond to equibiaxial tension (and stress states about), as was expected. Thus, the observed brittle behavior in less demanding applied stress states appeared to be accounted for as a result of residual stresses. Again, this result did not account for the larger brittle regime observed for the MSLC material. To explain this observation, we investigated the structure of the materials as described in the following sections.

Crystallinity

Crystallinity measurements were made via DSC and a density gradient column. DSC scans for the different extrusion rates are plotted in Figure 7(a) and are plotted for the different cooling rates in Figure 7(b). Crystallinity and T_m data from DSC and density and crystallinity values calculated from the density gradient column are presented in Table II. The agreement between the crystallinity values determined from the two methods was quite good. No significant change in crystallinity between samples was detected, except perhaps a slightly higher value for LSMC.

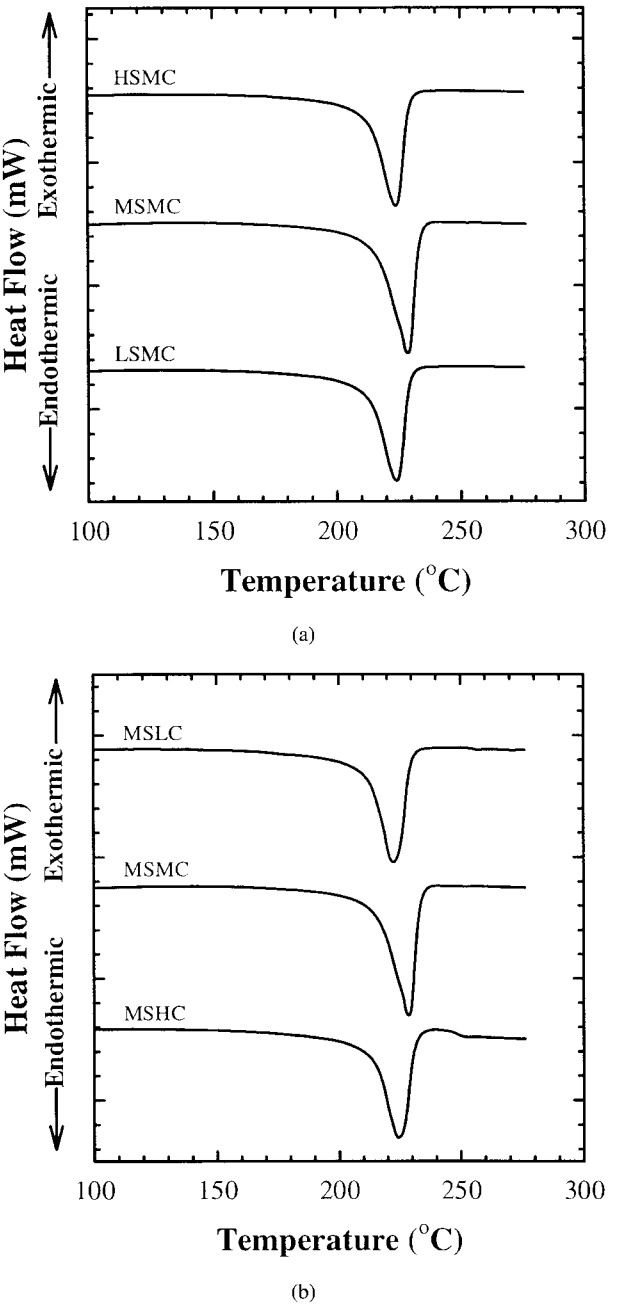

Figure 7 DSC scan of the materials processed at different (a) shear and (b) cooling rates. Heating rate = 10°C/min.

From the DSC results, it was also noticed that there was no significant difference in T_m between the samples or in the shape or width of the melting peaks. Qualitatively, this indicated similar values for the lamellar thickness or crystalline perfection for the samples. These results indicate that alterations in the shear or cooling rates had little effect on the crystalline phase of this material.

Table II T_m and Crystallinity Data from DSC and Density Gradient Column

Sample	Density (g/cm^3)	T_m (°C)	Crystallinity			
			DSC (wt %)		Density Column	
			10°C/min	2°C/min	Vol %	Wt %
MSMC	1.240	225	34	—	34	37
HSMC	1.240	224	33	—	34	37
LSMC	1.240	224	35	—	36	38
MSLC	1.240	223	33	38	34	37
MSHC	1.240	223	33	39	34	37

Because the mechanical behavior of this material did not change appreciably with change in shear rate, it was not surprising that few differences were observed for this case. However, it might be expected that the crystallinity of a slowly cooled material be higher than a rapidly cooled sample. Similarly, the degree of crystalline perfection and lamellar thickness would be expected to be greater. To study this more closely, we ran a second set of DSC runs on the MSLC and MSHC materials at a heating rate of 2°C/min, Figure 8. Again, no significant difference was found between the peaks or crystallinity values of the samples. In a previous study on this material, a MSMC sample was ground into a powder, melt-pressed, and quenched in liquid nitrogen.[16] The degree of crystallinity for this sample was determined to be 31%, compared to 34% for a sample cut directly from the cylinder. Thus, the quenching process did not greatly affect the crystallinity of this material. Because the cooling conditions used in production of the hollow cylinder samples that we received were not expected to be as severe as these, it seems reasonable that no differences in crystallinity were observed.

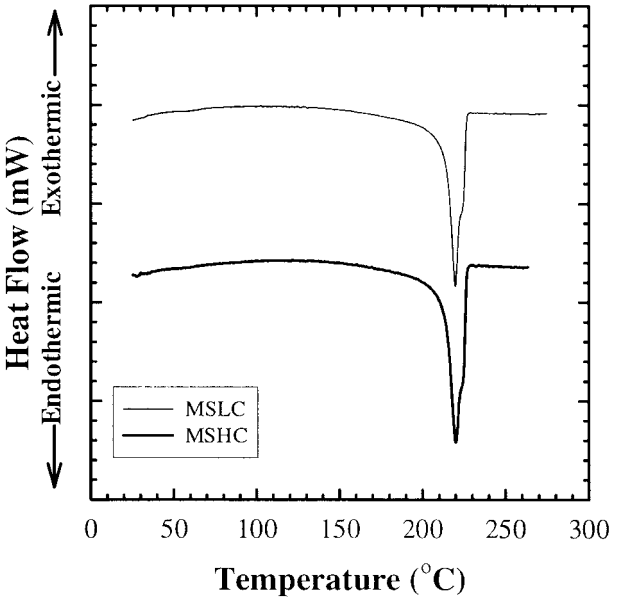

Figure 8 DSC scan of the materials processed at different cooling rates. Heating rate = 2°C/min.

It might also be expected that more tie molecules would be present in the MSHC material than in the MSLC material. This would result in greater ductility in comparison with the MSLC material, as observed. However, increased numbers of tie molecules should also lead to greater strength, which was not observed. Also, considering the rapid crystallization kinetics of the material[20,21] and the fact that the crystallinity values for the MSLC and MSHC materials were equivalent, it was not expected that crystal/amorphous segregation was more complete in one sample than the other.

Crystalline Orientation

WAXD patterns were obtained for all samples in the as-received condition. The diffraction patterns for the samples extruded at different rates are presented in Figure 9(a). The diffraction patterns for the samples processed with different cooling rates are presented in Figure 9(b). No significant crystalline orientation was detected in any of the samples. These patterns were obtained with the beam direction through the thickness of the cylinder. Patterns with the beam along the axial and tangential directions, although not presented here, were similar. Also, patterns obtained on the outer, "skin" layer indicated no crystalline orientation and appeared similar to those shown here.

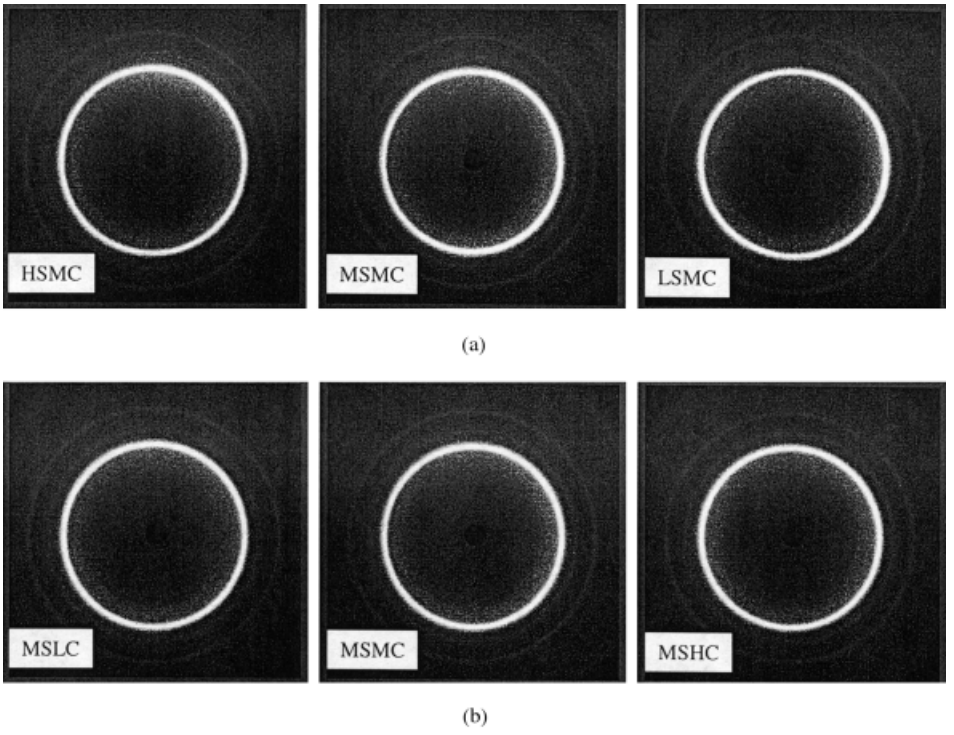

Figure 9 WAXD patterns for the samples processed at different (a) shear and (b) cooling rates. Beam direction is through the thickness of the samples.

For this material, the main diffraction peak was observed at $2\theta \sim 22°$. The width of this peak for each sample is compared in Figure 10(a,b). It can be seen from these figures that the peak widths were essentially equivalent. This indicates that the relative crystallite size for each sample was also equivalent. Thus, the WAXD results, similar to the DSC results, indicate that the altered processing conditions had no measurable effect on the crystalline phase of this material.

It was expected that some variation in crystalline phase orientation would be observed between the samples processed at different shear rates. However, this was not the case. Apparently very little, if any, orientation was present in the samples when crystallization initiated. This may mean that very little orientation was developed during melt flow, an observation also made by others in the case of iPP.[22] In that study, we performed wide-angle X-ray scattering on static and flowing melts to observe the changes in the scattering patterns due to shear-induced orientation. However, no differences were found between the static and flowing melts, indicating no presence of shear-induced structure.

Average Chain Orientation

This material was approximately 65% amorphous, and therefore, the amorphous phase was expected to play a significant role in the material behavior. To account for the presence of and possible orientation of this phase, ATR-IR spectra were obtained and analyzed for each sample. Although the phrase *amorphous orientation* may seem like an oxymoron, it is used within the context that *crystalline* suggests long-range order and that the amorphous component may have orientation within the short range.

Figure 11 contains representative spectra (MSMC material) and indicates the carbonyl peak that was analyzed. From the peak height values, an average angle of chain orientation was calculated for each sample. This angle was relative to the extrusion direction. Results are presented in Table III. The results indicated no significant level of orientation. The MSHC and HSMC samples showed orientation angles closer to the extrusion direction, as expected. Because no crystalline orientation was observed from the WAXD results, the detected orientation was assumed to be in the amorphous phase. Again, the results did

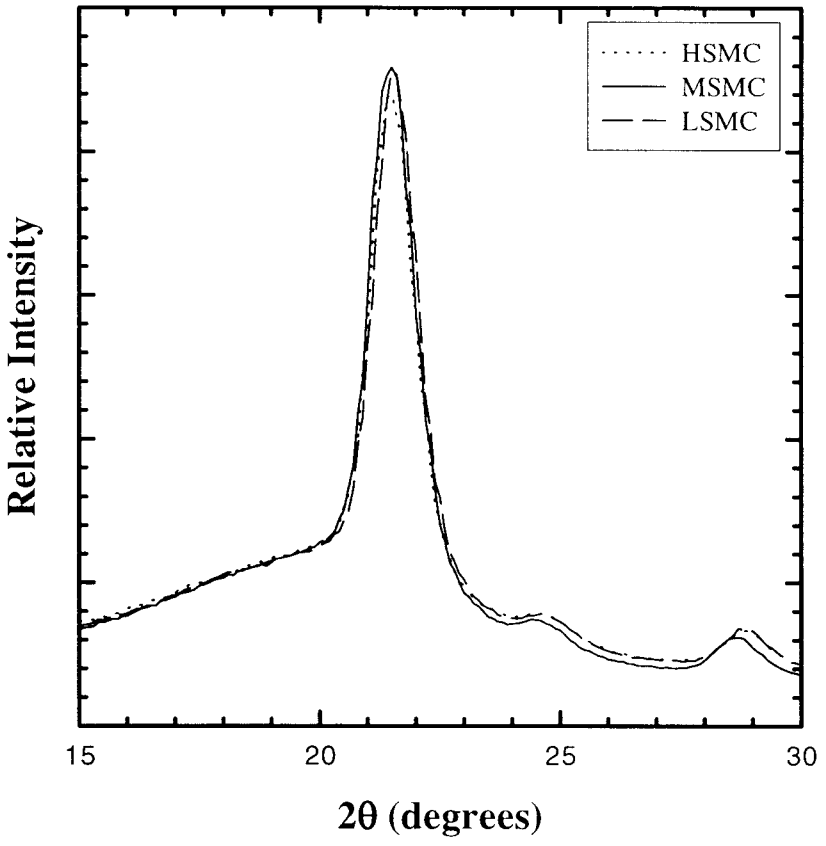

(a)

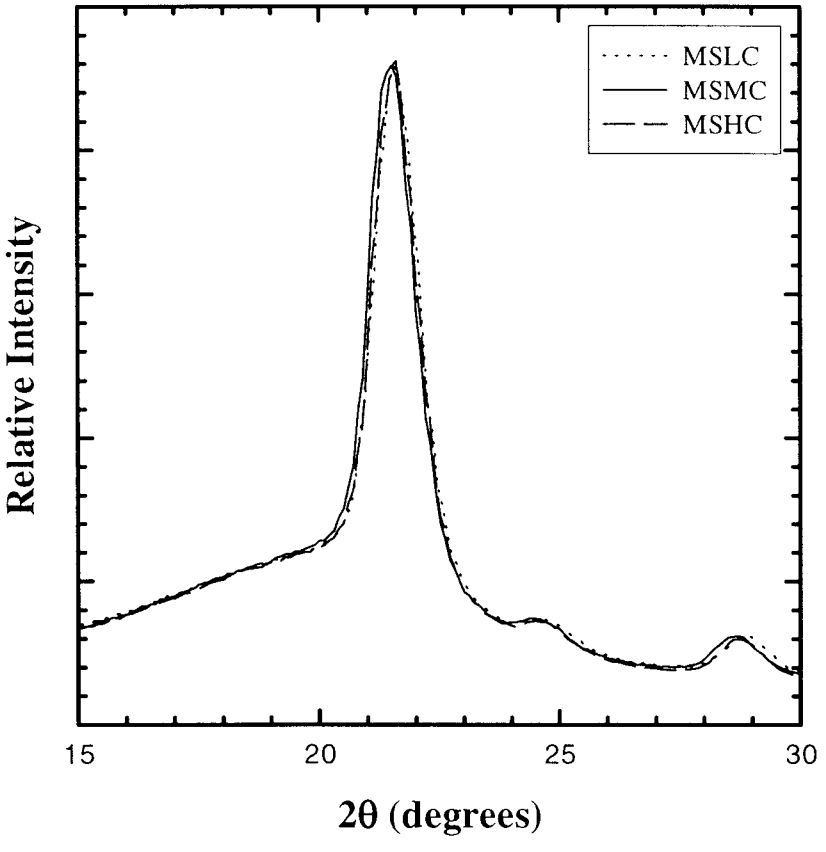

(b)

Figure 10 Main diffraction peak of the materials processed at different (a) shear and (b) cooling rates.

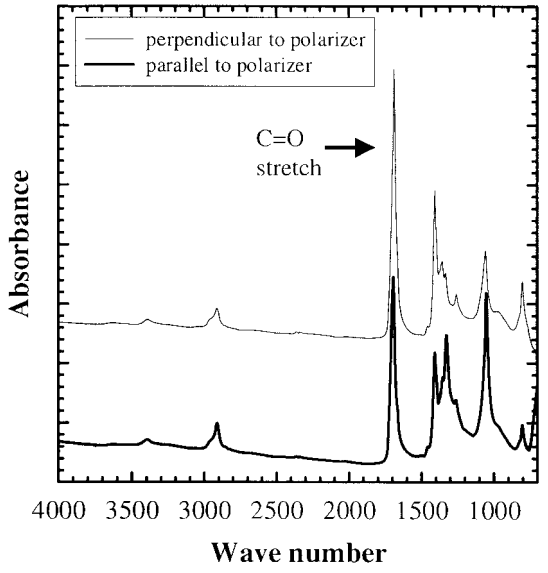

Figure 11 Representative IR spectra (MSMC material) with the extrusion direction oriented parallel and perpendicular with respect to the polarizer. Arrow indicates the peaks used in the analysis.

not give insight to the increased size of the brittle regime of the MSLC sample relative to the other samples. However, if the MSMC material was neglected (as explained previously), it did appear that the higher cooling rates and shear rates tended to preferentially orient the amorphous regions toward the axial direction.

Glass-Transition Temperature

As described previously, reported values for T_g for this material were in the 10–15°C range.[11,23] Because testing at 20°C is only slightly above this reported value, slight changes in the actual T_g value could impact the material behavior. Therefore, we questioned whether the processing conditions could affect this transition value or not. To determine if this was a factor in the brittle behavior of the MSLC material, we performed DMTA. Representative plots of tan δ as a function of temperature are shown in Figure 12(a,b). The mean transition temperatures are tabulated in Table IV. From these results, it is clear that the transition for our materials was higher than the reported values. The transition was also rather broad, span-

Table III Average Orientation Angles (with Respect to Extrusion Axis) as Determined from ATR-IR Spectra

Sample	Orientation Angle (°)
MSMC	46
HSMC	37
LSMC	45
MSLC	44
MSHC	35

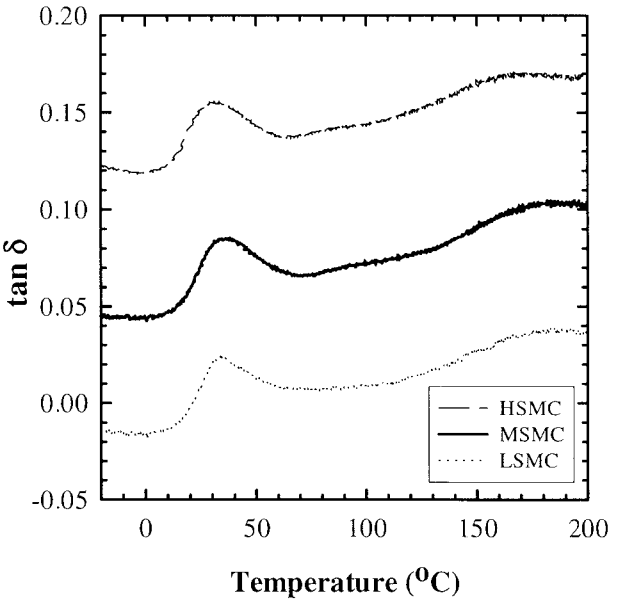

(a)

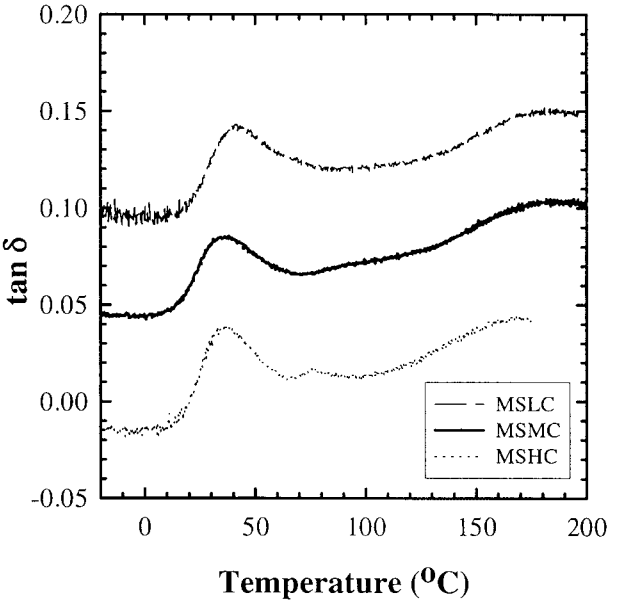

(b)

Figure 12 DMTA scans for samples processed at different (a) shear and (b) cooling rates.

Table IV Average T_g for Each Material

Sample	Average T_g (°C)
MSMC	32
HSMC	35
LSMC	31
MSLC	38
MSHC	36

ning roughly a 50°C temperature range. This was significant because testing was performed at 20°C—within this transition region.

It was expected that the more brittle MSLC material would have a slightly higher T_g than the other materials. However, within statistical error, all samples appeared to have similar T_g values Figure 13. Therefore, this transition probably had little effect on the difference in behavior between samples.

Spherulitic Structure

Electron micrographs for the MSMC, MSLC, and MSHC materials are presented in Figure 14. It is clear that the spherulite size in the MSMC material was much larger than in the other materials. This had originally been unexpected, as the morphology of this material was expected to be in between those of the MSLC and MSHC materials. This was explained by the fact that the MSMC material was processed at a separate location than the other four samples, as described previously. Therefore, other variables may have affected the morphology (different polymer batch, stabilizer package, etc.). Because of this, it was

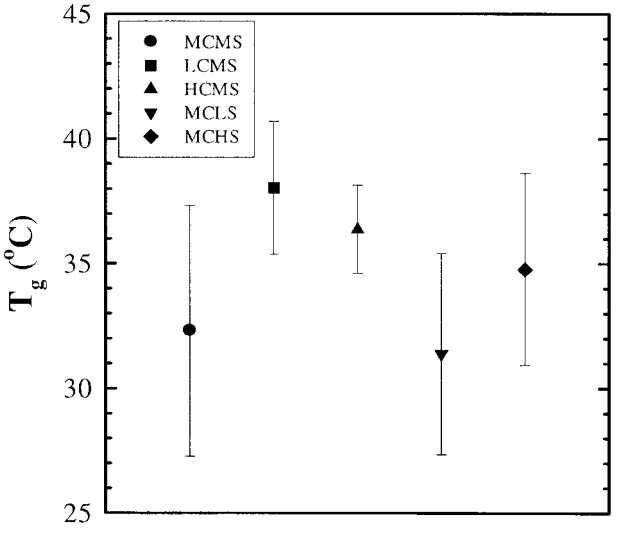

Figure 13 Average T_g for each sample as determined by DMTA, indicating error.

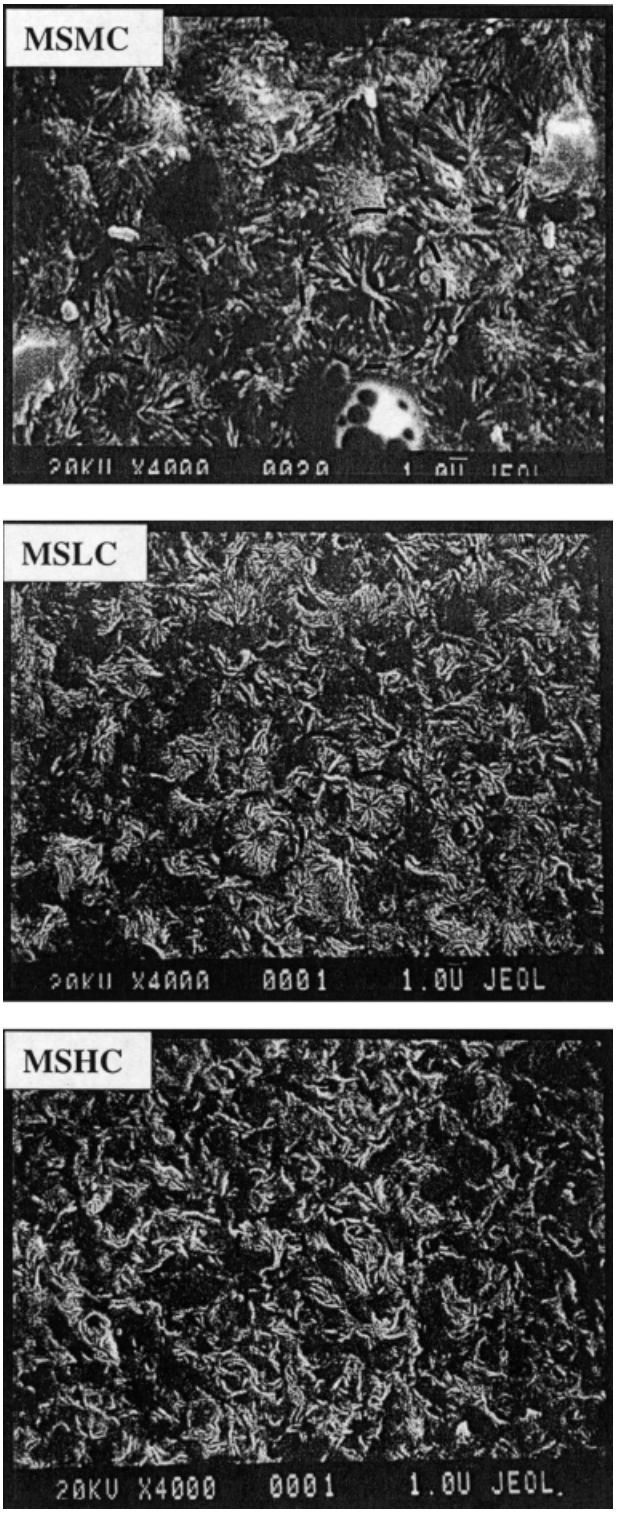

Figure 14 Electron micrographs for the MSMC, MSLC, and MSHC samples.

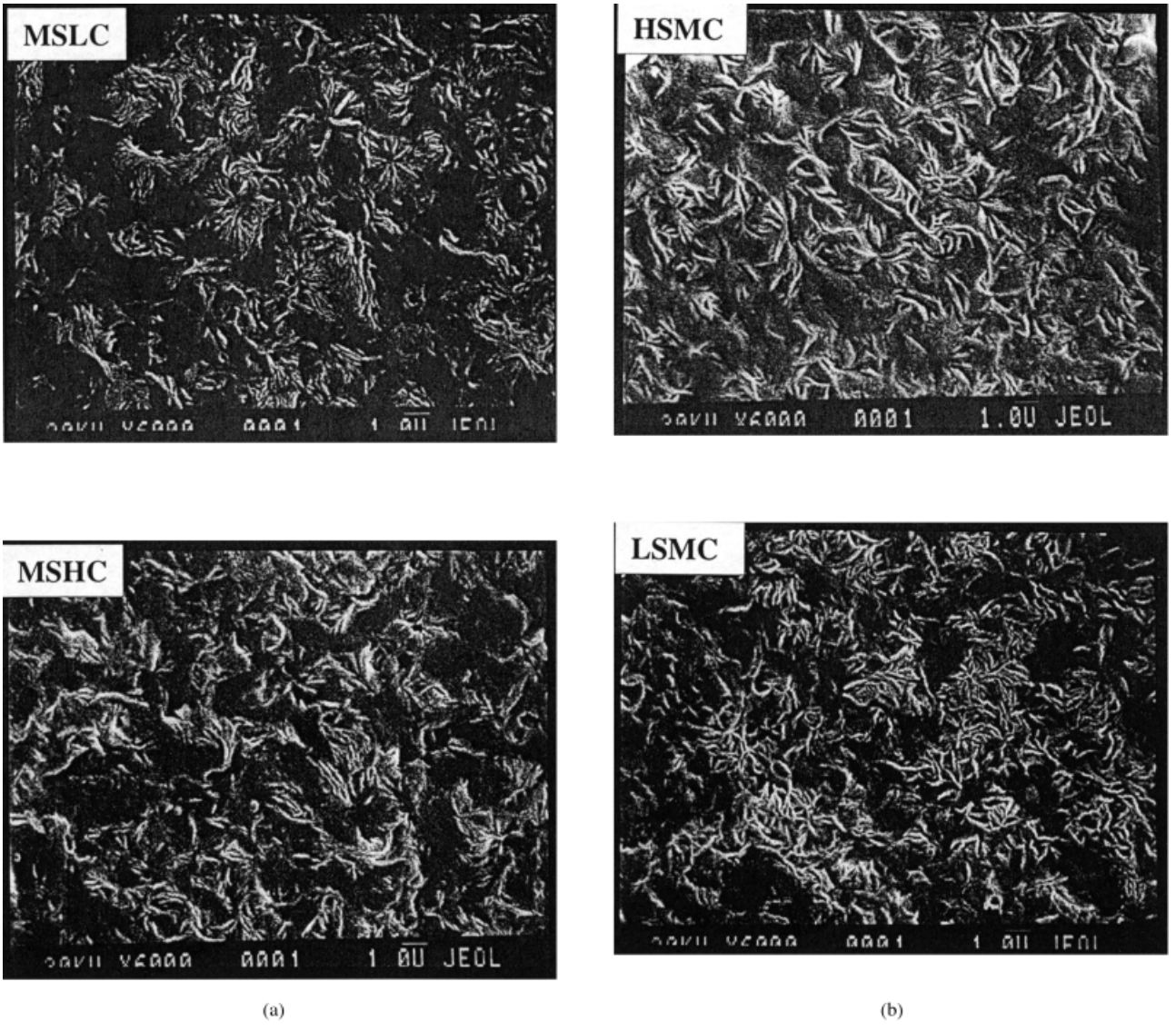

Figure 15 Electron micrographs for the HSMC, LSMC, MSLC, and MSHC samples.

not accurate to include this material in the comparison of the effects of processing conditions on the morphology of the aliphatic polyketone. It was, however, still possible to compare the remaining four samples.

Figure 15 indicates the micrographs for the MSLC, MSHC, HSMC, and LSMC materials at the same magnification. From these, a difference in the MSLC morphology can be seen. In this case, the spherulitic structure was rather distinct, allowing one to more readily identify individual spherulites than for the remaining three materials. In the case of the latter, the spherulitic structure appeared to be highly tangled or intertwined, making identification of individual spherulites more difficult. This could be partly responsible for the observed brittle behavior of the MSLC material, as it was the only distinguishing characteristic that was determined for this material.

CONCLUSIONS

Multiaxial testing was performed on hollow cylindrical samples of an aliphatic polyketone terpolymer that had been extruded with different shear and cooling rates. The morphological characteristics looked at included crystallinity, lamellar thickness, crystalline orientation, overall orienta-

tion, morphology, and T_g. The effects of shear rate on the mechanical behavior and morphological characteristics were negligible, except for slight differences in overall orientation. The cooling rate, on the other hand, had significant effects on the yield behavior of this material. The slowly cooled material displayed more brittle behavior than the standard or rapidly cooled sample. Although clear differences in failure behavior were observed, morphological differences were very difficult to detect with any of the techniques used. Some differences that could be detected were slight differences in overall orientation and a more defined spherultic structure for the sample cooled at a lower rate. An important factor may have been the broad glass transition. Testing at 20°C, although originally thought to be above the T_g, was determined to take place within the transition range and, therefore, could have affected the behavior of the material.

Ductile behavior was observed for the loading condition of biaxial–biaxial tension for all samples except the slowly cooled material. This was in contrast to what was expected because this stress state was the most demanding. The observation seems to be explained by the presence of residual stresses, which effectively shifted the stress state felt by the material.

The authors would like to thank Professor Shaw Hsu and Dr. Andrei Stolov for their ATR-IR expertise and Dr. Alan Waddon for his helpful consultation. They also thank Dr. James Kau and Shell Chemical Co. for materials and financial support.

REFERENCES

1. Mathew, B. A.; Nunn, R. E.; Orroth, S. A. Polym Mater Sci Eng 1988, 59, 1212.
2. Lagasse, R. R.; Maxwell, B. Polym Eng Sci 1976, 16, 189.
3. Greco, R.; Coppola, F. Plast Rubber Proc Appl 1986, 6, 35.
4. Macauley, N. J.; Harkin-Jones, E. M. A.; Murphy, W. R. Polym Eng Sci 1998, 38, 662.
5. Ohlberg, S. M.; Roth, J.; Raff, R. A. V. J Appl Polym Sci 1959, 1, 114.
6. Starkweather, J Appl Polym Sci 1959, 1, 236.
7. Broutman, L. J.; Krishnakumar, S. M. Polym Eng Sci 1976, 16, 74.
8. So, P.; Broutman, L. J. Polym Eng Sci 1976, 16, 785.
9. Gerlowski, E. L.; Kastelic, J. R. U.S. Pat. 5,077,385 (1990).
10. Del Nobile, M. A.; Mensitieri, G.; Sommazzi, A. Polym 1995, 36, 4943.
11. Flood, J. E.; Weinkauf, D. H.; Londa, M. In 53rd ANTEC; 1995; Vol. 2, p 2326.
12. Karttunen, N. R.; Lesser, A. J. J Mat Sci 2000, 35, 2507.
13. Clutton, E. Q.; Williams, J. G. Polym Eng Sci 1995, 35, 1381.
14. Lommerts, B. J.; Klop, E. A.; Aerts, J. J Polym Sci Part B: Polym Phys 1993, 31, 1319.
15. Klop, E. A.; Lommerts, B. J.; Veurink, J.; Aerts, J.; Van Puijenbroek, R. R. J Polym Sci Part B: Polym Phys 1995, 33, 315.
16. Waddon, A. J.; Karttunen, N. R.; Lesser, A. J. Macromolecules 1999, 32, 423.
17. Shkrabo, D. M.; Zhizhin, G. N.; Kuzik, L. A.; Garbuzova, I. A. Vibrational Spectr 1998, 17, 155.
18. Koenig, J. L. In Spectroscopy of Polymers; American Chemical Society: Washington DC, 1992.
19. Jones, N. A.; Lesser, A. J. J Polym Sci Part B: Polym Phys 1998, 37, 3246.
20. Holt, G. A., Jr.; Spruiell, J. E. In 54th ANTEC; 1996; Vol. 2, p 1780.
21. Holt, G. A., Jr.; Spruiell, J. E. Polym Mater Sci Eng 1997, 76, 112.
22. Hendra, P. J.; Taylor, M. A.; Willis, H. A. J Polym Sci Part C: Polym Lett 1986, 24, 83.
23. Ash, C. Int J Polym Mater 1994, 30, 1.